Supplementary Materials for

Crystal structure of a heterotetrameric NMDA receptor ion channel

Erkan Karakas, Hiro Furukawa*

*correspondence to: furukawa@cshl.edu

This PDF file includes:

Materials and Methods
Figs. S1 to S16
Table S1

Materials and Methods

Construct Design

The genes encoding the C-terminally truncated rat GluN1a (residues 1-847, accession code: P35439) and GluN2B (residues 27-852, accession code: Q00960), which is C-terminally truncated and N-terminally fused to GluN1 signal peptide, OneStrep tag and a thrombin recognition site, were cloned into pUCDM and pFL vectors, respectively (*39*). Polyhedrin promoter in the original vectors was replaced by Hsp70 promoter. Those two plasmids were recombined using Cre recombinase as described previously (*39*). To improve crystal quality of GluN1a/GluN2B NMDA receptors, the following mutations were initially incorporated: 1) 6 out of 11 putative glycosylation sites on GluN1a and 1 out of 6 putative glycosylation sites on GluN2B were removed by mutations on GluN1a (Asn61Gln, Asn239Asp, Asn350Gln, Asn471Gln, Asn491Gln and Asn771Gln) and on GluN2B (Asn348Asp); 2) cysteine residues, Cys22 on GluN1a and Cys588, Cys838 and Cys849 on GluN2B were mutated to serine to avoid non-specific disulfide bond formation; 3) six residues, Cys395, Pro396, Glu397, Glu399, Glu400 and Glu402, were removed from the ATD-LBD linker on GluN2B; and 4) patches of charged residues on the cytoplasmic loop of GluN1a was neutralized by mutations, Glu594Gln, Glu595Ser, Glu597Ser, Glu598Thr, Arg844Asn, Arg845Gly and Lys846Ala. This construct, GluN1a/GluN2B$_{cryst}$, crystallized and resulted in 5.7 Å resolution structure. Based on the structure, GluN1a/GluN2B$_{crystx}$ construct was designed and made by introducing the GluN2B Ser214Cys mutation to cross-link the two GluN2B ATDs and GluN1a-Thr561Cys/GluN2B-Ile815Cys and GluN1a-Phe810Cys/GluN2B-Asp557Cys mutation pairs at the TMD to further stabilize the heterotetramer.

Expression and purification

Large scale expression of GluN1a/GluN2B$_{crystx}$ NMDA receptors were performed by infecting *Sf9* insect cells at a cell density of 4 x 10^6 cells/ml using baculovirus harboring both GluN1a$_{crystx}$ and GluN2B$_{crystx}$ genes under the control of HSP70 promoter from *Drosophila melanogaster*. At 48 hours post infection, cells were harvested by centrifugation at 1,000 g for 20 min. and lysed in a buffer composed of 150 mM NaCl, 20 mM HEPES-NaOH pH 7.3 and 1 mM phenylmethylsulphonyl fluoride (PMSF) using Avestin EmulsiFlex-C5. The cell lysate was centrifuged at 6,000 g for 25 minutes and the membrane was pelleted by centrifugation at 185,000 g for 1 hour. The membranes were homogenized and solubilized in 180 mM NaCl, 40 mM HEPES-NaOH pH 7.3 and 0.5% lauryl maltose neopentyl glycol (MNG-3) for 3 hours, prior to centrifugation at 185,000 g for 40 minutes to remove insoluble materials. The GluN1a/GluN2B$_{crystx}$ proteins in the supernatant were loaded onto Strep-tactin Superflow, washed with 15 column volumes of the wash buffer composed of 500 mM NaCl, 20 mM HEPES-NaOH pH 7.3, 0.01% MNG-3 and 0.01 mg/ml 1-palmitoyl-2-oleoyl-sn-glycero-3-phosphocholine (POPC), and eluted with the same buffer containing 3 mM d-desthiobiotin. Following thrombin digestion to remove the strep tag at 18°C overnight, protein was further purified by size exclusion chromatography using Superose 6 (10/300 GL, GE Healthcare) equilibrated with 200 mM NaCl, 20 mM HEPES-NaOH pH 7.3, 0.01% MNG-3 and 0.01 mg/ml POPC at room temperature. The fractions that correspond to GluN1a/GluN2B$_{crystx}$ were concentrated to 4.5-5 mg/ml, supplemented with 10 mM glycine, 10 mM L-glutamate

and 0.1 mM ifenprodil and used for crystallization immediately. To produce SeMet-incorporated GluN1a/GluN2B$_{crystx}$ proteins, the culture medium was substituted with methionine free ESF921 media prior to viral infection. After one hour, L-SeMet at 75 mg/L was added to the culture and the media was harvested 48 h post infection. The proteins were purified as described above.

Crystallization

Crystals of GluN1a/GluN2B$_{cryst}$ NMDA receptors were initially obtained by vapor diffusion using a reservoir solution of 15% PEG 4000, 0.1 M Tris-HCl (pH 8.5) and 0.2 M $MgCl_2$ (MembFac, Hampton Research). However, the diffraction was limited to 8.0 Å after extensive optimization of the crystallization conditions. Use of $Mg(OAc)_2$ instead of $MgCl_2$ dramatically increased crystal size by 3 fold and increased the diffraction power to ~7.0 Å. Diffraction power was further improved by including synthetic lipids, POPC, in purification buffers and incubating crystals in 1 M $Mg(OAc)_2$ containing buffer, which also acted as cryo-protectant, for 24 hours prior to flash freezing. The most dramatic improvement was observed on crystals soaked with the heavy atom cluster, hexa-sodium metatungstate, where diffraction reached up to 5.7 Å. At this point, we were able to obtain a structure of GluN1a/GluN2B$_{cryst}$ NMDA receptor by molecular replacement as described below. This low resolution structure was used to design cross-linking mutations to stabilize the tetramer. After extensive screening of cross-link constructs for crystallization and x-ray diffraction, the GluN1a/GluN2B$_{crystx}$ (described above) yielded crystals that diffracted beyond 4.0 Å. The best diffracting crystals of GluN1a/GluN2B$_{crystx}$ NMDA receptor were obtained by vapor diffusion at 18 °C in hanging drops containing 1.4 µl of protein solution, 0.5 µl of reservoir solution (10-12% PEG 4000, 0.2 M NaCl, 0.1 M Tris-HCl pH 8.8 and 0.4 M $Mg(OAc)_2$), and 0.4 µl of 0.1 mM hexa-sodium metatungstate. Crystals were first incubated in a buffer containing 12% PEG 4000, 0.08 M Tris-HCl pH 8.8, 0.02 M HEPES-NaOH pH 7.3, 0.2 M NaCl, 1 M $Mg(OAc)_2$, 0.01% MNG-3, 10 mM glycine, 10 mM L-glutamate, 0.1 mM ifenprodil, 0.01 mg/ml POPC, and 0.05 mM hexa-sodium metatungstate for 24 hours and flash frozen by liquid nitrogen after soaking in the same buffer but with higher hexa-sodium metatungstate concentration (1 mM) for 2 hours. Holmium and gadolinium derivatives were obtained by including 100 mM $HoCl_3$ or $GdCl_3$ in the final soaking buffer.

Data collection and structure determination

Data collection was performed using synchrotron radiation at the beamlines ID23-B and ID23-D at the Advanced Photon Source (APS) at Argonne National Laboratory and at the beamline BL41XU at SPring-8. Datasets were indexed, integrated and scaled using HKL2000 (*40*). Diffraction power of the datasets collected from single crystals was limited to 4.2 Å due to radiation damage. Therefore, datasets collected from 15 different crystals of GluN1a/GluN2B$_{crystx}$ construct were indexed and integrated separately and scaled together using HKL2000 (*40*). The structure was solved by molecular replacement using the coordinates of GluN1b/GluN2B ATD (PDB code: 3QEL) (*7*) and GluN1/GluN2B LBD model built based on the GluN1/GluN2A LBD structure (PDB code: 2A5T) (12) with the program PHASER (*41*). The model was built using COOT (*42*) and initial structural refinement was performed using jellybody refinement implemented in the program REFMAC (*16*) along with PROSMART (*43*) to create

restraints based on the high resolution structures of the isolated ATD and LBD structures and using deformable elastic network (DEN) refinement (*17*). Final refinement cycles were performed using Phenix (*44*) with restraints based on two-fold non-crystallographic symmetry, secondary structure and high resolution structures of ATD and LBDs.

Cysteine cross-linking and western blot

Proteins with incorporated cysteine mutations on GluN1a/GluN2B$_{cryst}$ constructs were expressed as described above. Harvested cell pellets were solubilized in a buffer composed of 150 mM NaCl, 20 mM HEPES-NaOH pH 7.3, 0.5% MNG-3, 10 mM glycine, 10 mM L-glutamate, 0.01 mM ifenprodil and 1mM PMSF and centrifuged at 185,000g. The GluN1a/GluN2B proteins in the supernatant were purified using Strep-tactin Superflow resin and subjected to SDS-polyacrylamide gel electrophoresis (7%) in the presence and absence of 150 mM β-mercaptoethanol. The proteins were transferred to Hybond-ECL nitrocellulose membranes (GE Healthcare). The membrane was blocked with 5% milk in TBST (20 mM Tris-HCl pH 8.0, 150 mM NaCl and 0.05% Tween-20), then incubated with mouse monoclonal antibodies against GluN1 (MAB1586, Millipore) or GluN2B (ab93610, Abcam), followed by HRP-conjugated anti-mouse antibodies (GE Healthcare). Protein bands were detected by ECL detection kit (GE Healthcare).

Electrophysiology

Recombinant GluN1a/GluN2B NMDA receptors were expressed by co-injecting 0.1-0.5 ng of the wild-type or mutant rat GluN1a and GluN2B cRNAs at a 1:2 ratio (w/w) into defolliculated *Xenopus laevis* oocytes. The two-electrode voltage-clamp recordings were performed using agarose-tipped microelectrodes (0.4-1.0 MΩ) filled with 3 M KCl at a holding potential of -60 mV. The bath solution contained 5 mM HEPES, 100 mM NaCl, 0.3 mM $BaCl_2$ and 10 mM Tricine at pH 7.4 (adjusted with KOH). Currents were evoked by applications of 100 μM of glycine and L-glutamate and potentiated or allosterically inhibited by spermine and ifenprodil, respectively. Whole-cell patch-clamp recordings were performed on HEK 293 cells transfected with GluN1a$_{cryst}$ in pUCDM and GluN2B$_{cryst}$ in pFL under CMV promoter. All of the recordings were done at −60 mV (23 °C) with micropipettes containing (in mM) 110 D-gluconate, 110 CsOH, 30 CsCl, 5 HEPES, 4 NaCl, 0.5 $CaCl_2$, 2 $MgCl_2$, 5 BAPTA, 2 NaATP and 0.3 NaGTP (pH 7.35). The external solution contained (in mM) 150 NaCl, 10 HEPES, 30 D-mannitol, 3 KCl, 1.0 $CaCl_2$ and 0.01 EDTA at 23°C and pH 7.4. Rapid solution exchange was accomplished with a piezoelectric driven two barreled theta glass pipette (Burleigh Instruments, Newton NJ); typical 10-90% exchange times for solutions around the cells were < 3ms. Deactivation and desensitization time course were fitted with the double exponential equation: Response = $Amplitude_{FAST}$ (exp(-time/tau_{FAST})) + $Amplitude_{SLOW}$(exp(-time/tau_{SLOW}). Data acquisition was performed with pClamp version 9-10 and analysis performed using Channelab.

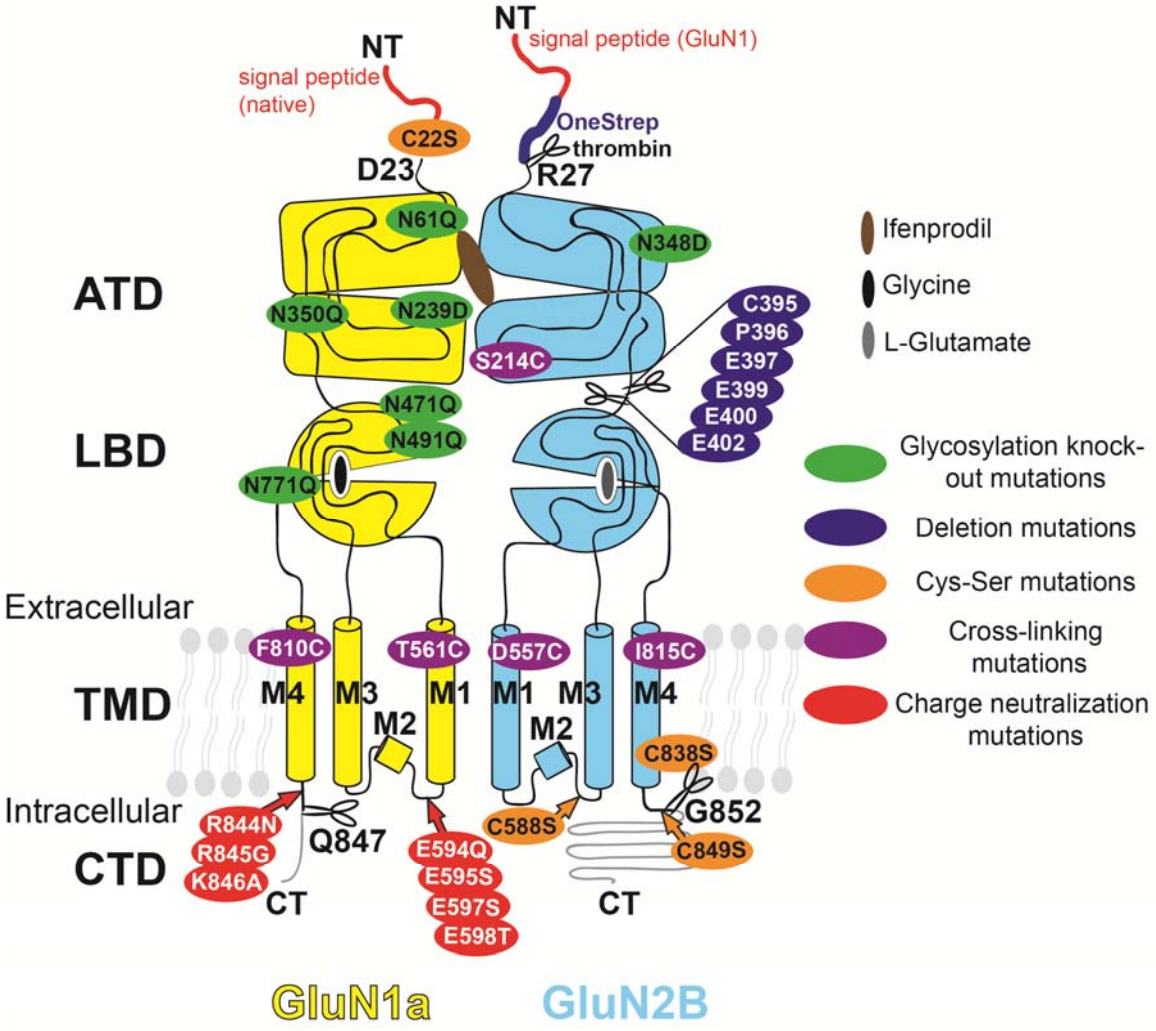

Fig. S1. Construct design of NMDA receptor subunits. Schematic representation of rat GluN1a$_{crystx}$ (yellow) and GluN2B$_{crystx}$ (cyan) subunits highlighting the modification performed on both constructs. Amino terminal domain (ATD), ligand binding domain (LBD), transmembrane domain (TMD) and carboxy terminal domain (CTD) for both subunits are shown as separate domains. The GluN1a subunit is truncated at the C-terminus (Gln 847) and expressed with the native signal peptide. C-terminally truncated GluN2B subunit is fused to the signal peptide from GluN1a, OneStrep tag, and a thrombin recognition site at the N-terminus (Arg 27). Mutations to remove predicted glycosylation sites are highlighted in green. Cysteine to serine mutations to avoid non-specific disulfide bond formation are shown in orange and residues that are removed from the ATD and LBD linker on GluN2B subunits are shown in blue. Point mutations to neutralize the charged groups of residues at the cytoplasmic side of GluN1a subunit are indicated in red. To stabilize the tetrameric arrangement of the NMDA receptor, cysteine mutations (purple) are introduced to cross-link M1 helices to the M4 helices of the neighboring subunits at the TMD and the two GluN2B ATDs.

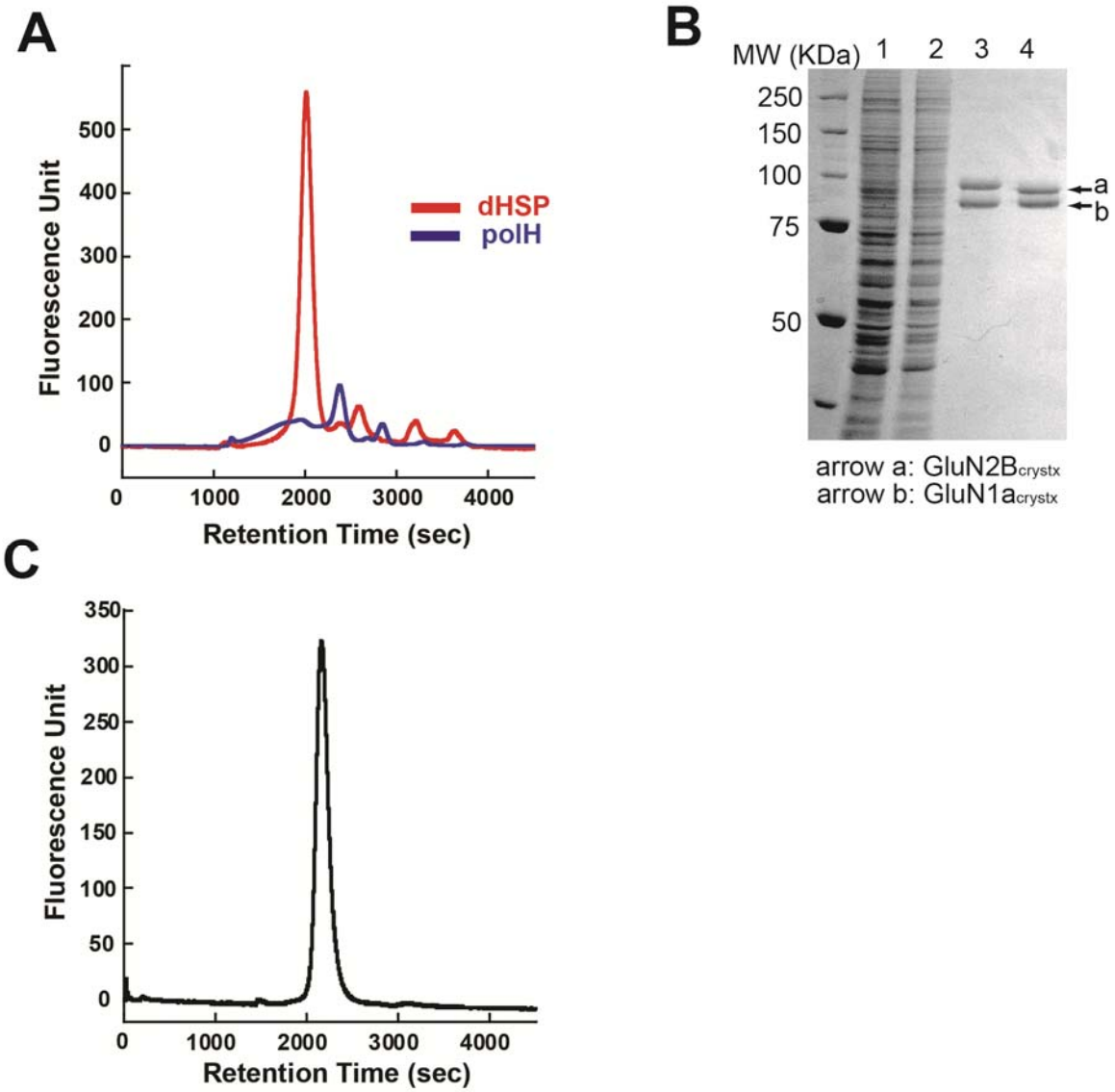

Fig. S2: Expression and purification of GluN1a/GluN2B NMDA receptors. (A) GluN1a$_{cryst}$ that is fused to EGFP at the C-terminal end is co-expressed with GluN2B$_{cryst}$ in *Sf9* insect cells under heat-shock protein promoter from *Drosophila melanogaster* (red, dHSP) or polyhedrin promoter (blue, polH) using baculovirus. The GluN1a$_{cryst}$-EGFP/GluN2B$_{cryst}$ NMDA receptor proteins are extracted by MNG-3 and detected by fluorescence coupled size exclusion chromatography (FSEC) (475 nm excitation/507 nm emission) (*48*). The major peak at the retention time of ~2,000 second for the sample expressed under dHSP represents heterotetramers. Such peak is almost absent when the proteins are expressed under polH. **(B)** Purification of GluN1a/GluN2B$_{crystx}$ NMDA receptor proteins from insect cells using Strep-tactin Superflow. SDS-PAGE showing MNG-3 solubilized material (lane 1), flow through fraction from the column (lane 2), the elution fraction (lane 3), and the elution fraction treated with thrombin to remove OneStrep tag fused to GluN2B$_{crystx}$ (lane 4). **(C)** Size exclusion chromatogram of purified GluN1a/GluN2B$_{crystx}$ NMDA receptor proteins detected by intrinsic tryptophan fluorescence (280 nm excitation/330 nm emission).

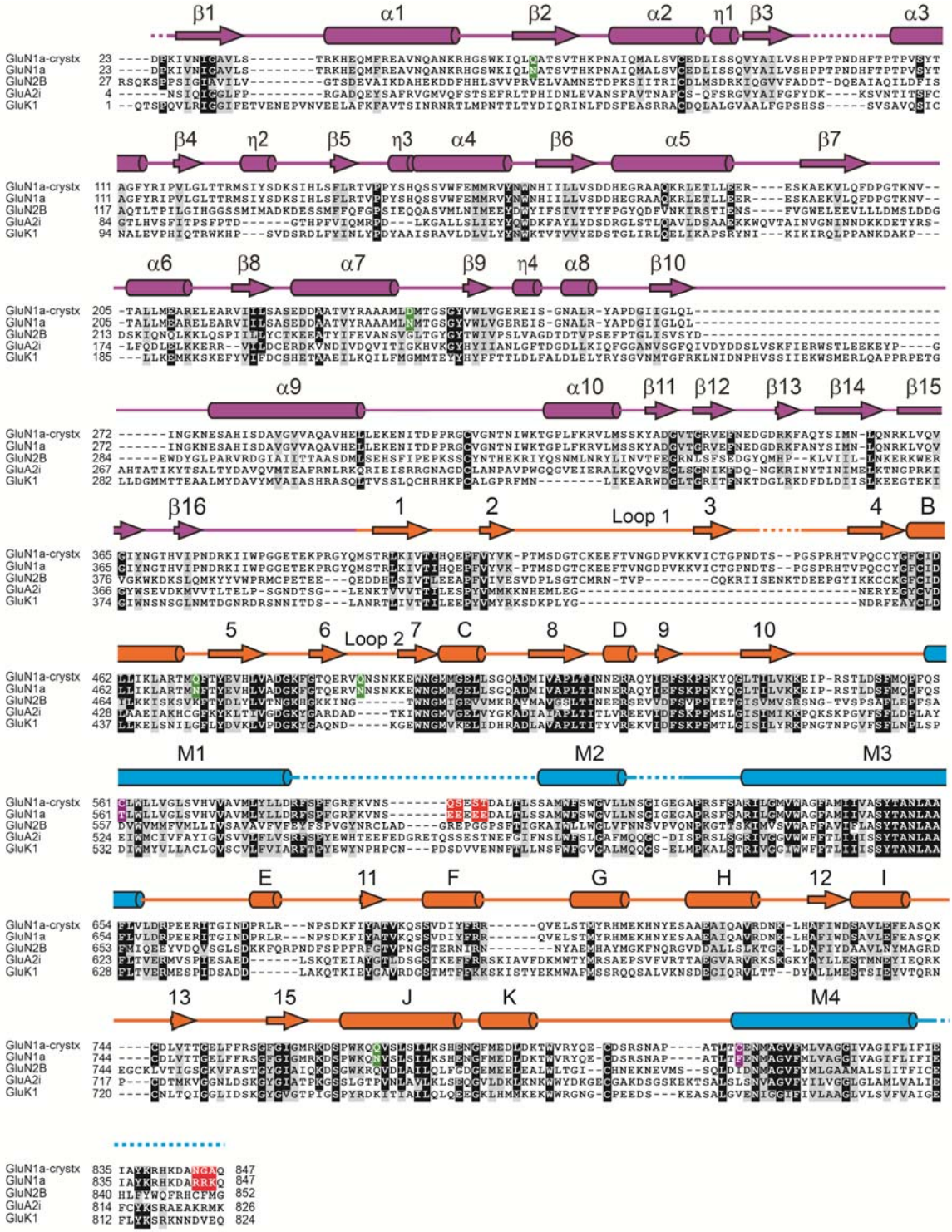
β1 α1 β2 α2 η1 β3 α3
β4 η2 β5 η3 α4 β6 α5 β7
α6 β8 α7 β9 η4 α8 β10
α9 α10 β11 β12 β13 β14 β15
β16 1 2 Loop 1 3 4 B
5 6 Loop 2 7 C 8 D 9 10
M1 M2 M3
E 11 F G H 12 I
13 15 J K M4
GluN1a-crystx
GluN1a
GluN2B
GluA2i
GluK1

Fig. S3: Multiple sequence alignment of GluN1a$_{crystx}$ with other ionotropic glutamate receptor subunits. Shown here are the primary sequences of GluN1a$_{crystx}$, rat GluN1a (P35439), rat GluN2B (Q00960), rat GluA2i (NP_058957) and GluK1 (P22756_2). Sequences for the C-terminal domain are excluded from the alignment. The sequence alignment is annotated with arrows for β-strands, cylinders for α- and η (3_{10})-helices and lines for loops based on the crystal structure of GluN1a$_{crystx}$. The structural annotation is colored according to domains as magenta (ATD), orange (LBD) and cyan (TMD). Disordered regions with no clear electron density are shown as dashed lines. The names of the helices and strands are kept the same as in high resolution structures of isolated GluN1b/GluN2B ATD (α, η and β prefixed) and GluN1/GluN2A LBD (capital letters and numbers). Mutated residues are highlighted with the same color code as in Fig. S1.

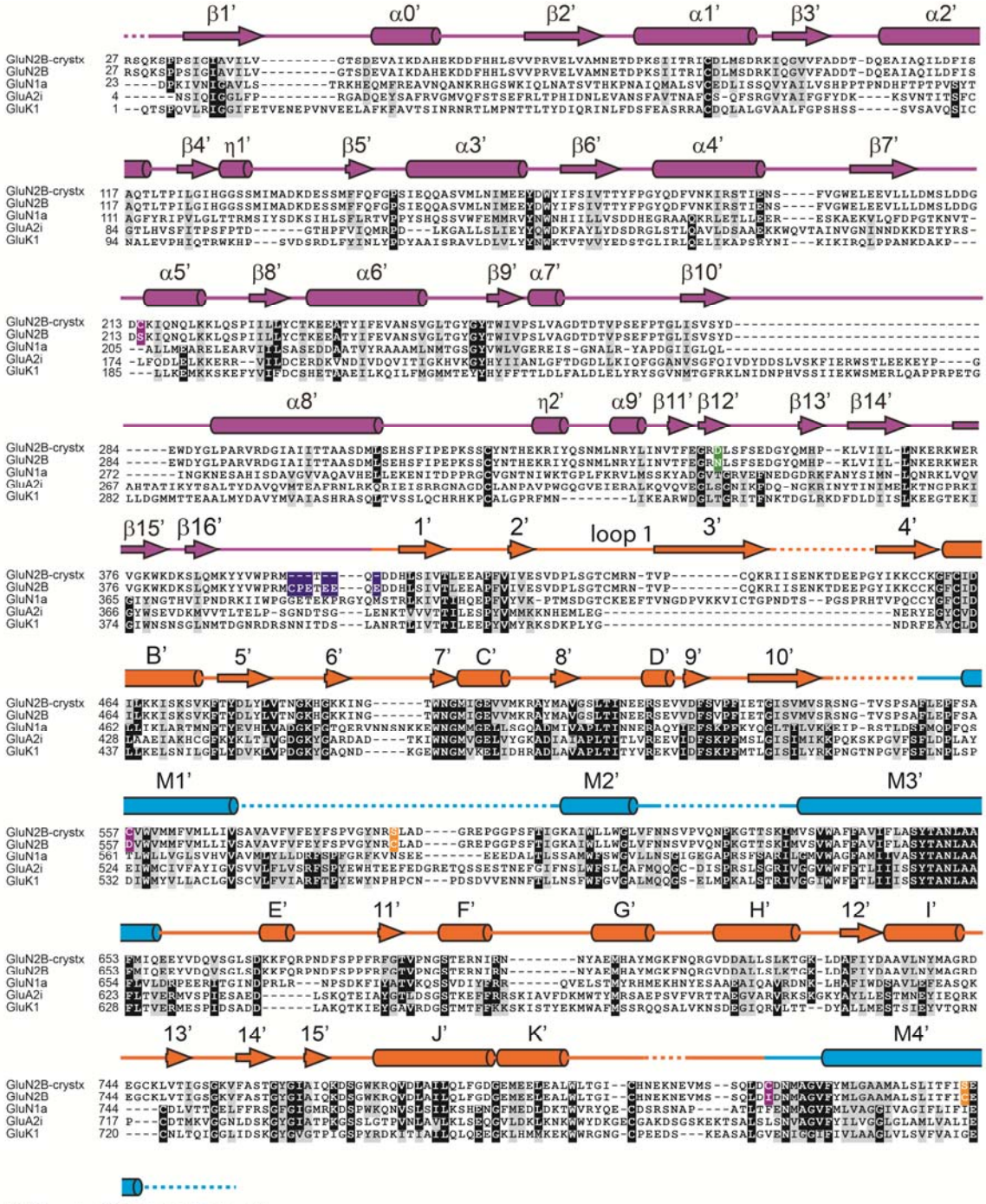
β1' α0' β2' α1' β3' α2'
GluN2B-crystx
GluN2B
GluN1a
GluA2i
GluK1
β4' η1' β5' α3' β6' α4' β7'
α5' β8' α6' β9' α7' β10'
α8' η2' α9' β11' β12' β13' β14'
β15' β16' 1' 2' loop 1 3' 4'
B' 5' 6' 7' C' 8' D' 9' 10'
M1' M2' M3'
E' 11' F' G' H' 12' I'
13' 14' 15' J' K' M4'

Fig. S4: Multiple sequence alignment of GluN2B$_{crystx}$ with ionotropic glutamate receptors. Shown here are the primary sequences of GluN2B$_{crystx}$, rat GluN2B (Q00960), rat GluN1a (P35439), rat GluA2i (NP_058957) and GluK1 (P22756_2). Sequences for the C-terminal domain are excluded from the alignment. The sequence alignment is annotated with arrows for β-strands, cylinders for α- and η (3_{10})-helices and lines for loops based on the crystal structure of GluN2B$_{crystx}$. The structural annotation is colored according to domains as magenta (ATD), orange (LBD) and cyan (TMD). Disordered regions with no clear electron density are shown as dashed lines. The names of the helices and strands are kept the same as in high resolution structures of isolated GluN1b/GluN2B ATD (α, η and β prefixed) and GluN1/GluN2A LBD (capital letters and numbers). Mutated residues are highlighted with the same color code as in Fig. S1.

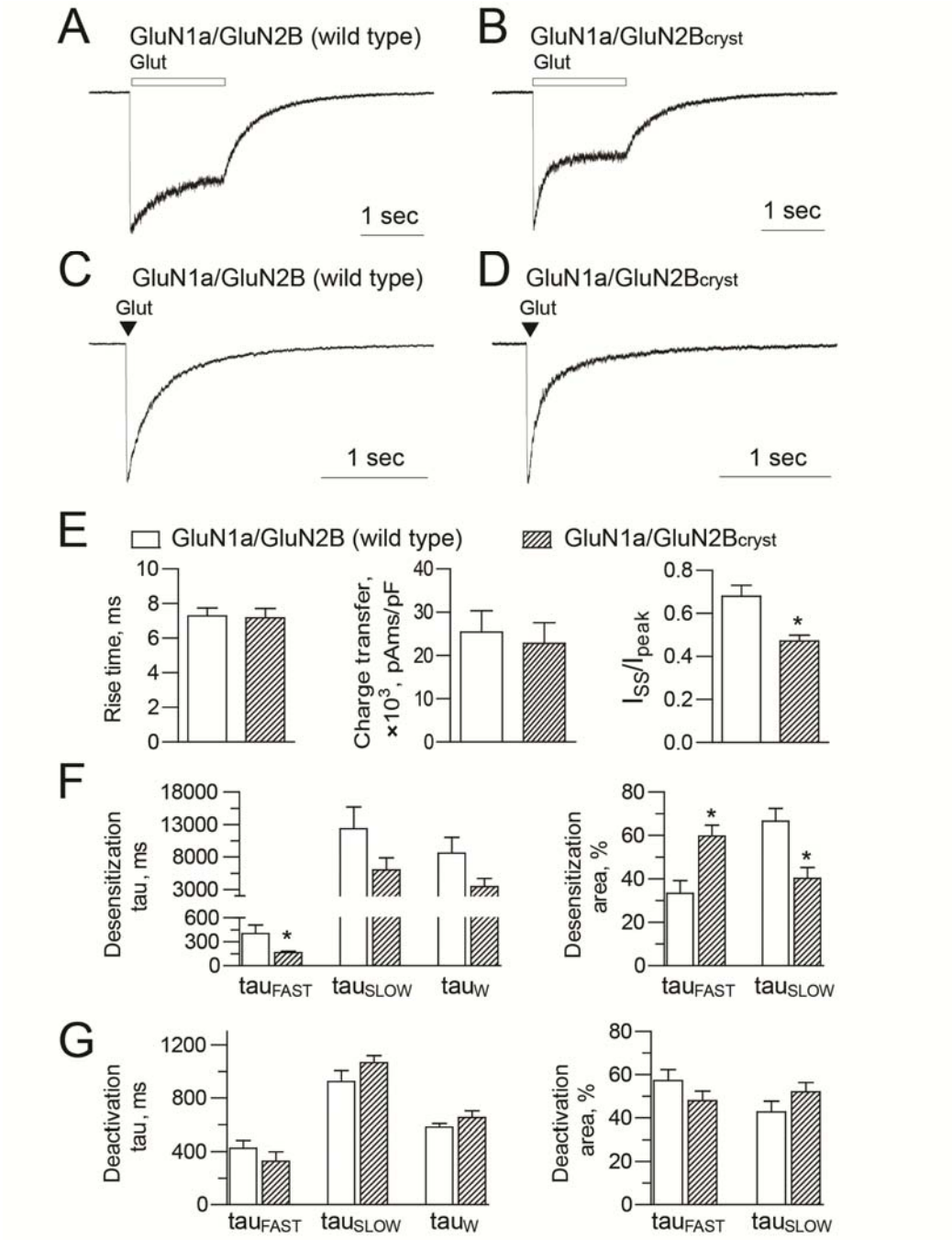

Fig. S5: Electrophysiological measurement of the response time course of mutant GluN1a/GluN2B NMDA receptors. (A-D) Representative whole cell patch-clamp recordings of wild-type GluN1a/GluN2B (**A** and **C**) and GluN1a/GluN2B$_{cryst}$ (**B** and **D**) expressed in HEK293 cells and activated with long (**A** and **B;** 1.5 sec) and brief (**C** and **D;** 5 msec) application of 1 mM glutamate in the constant presence of 100 µM glycine. The cells were voltage-clamped at −60 mV. (**E-G**) Comparison of time courses for activation **(E)**, desensitization **(F)**, and deactivation **(G)** of wild-type GluN1a/GluN2B and GluN1a/GluN2B$_{cryst}$.

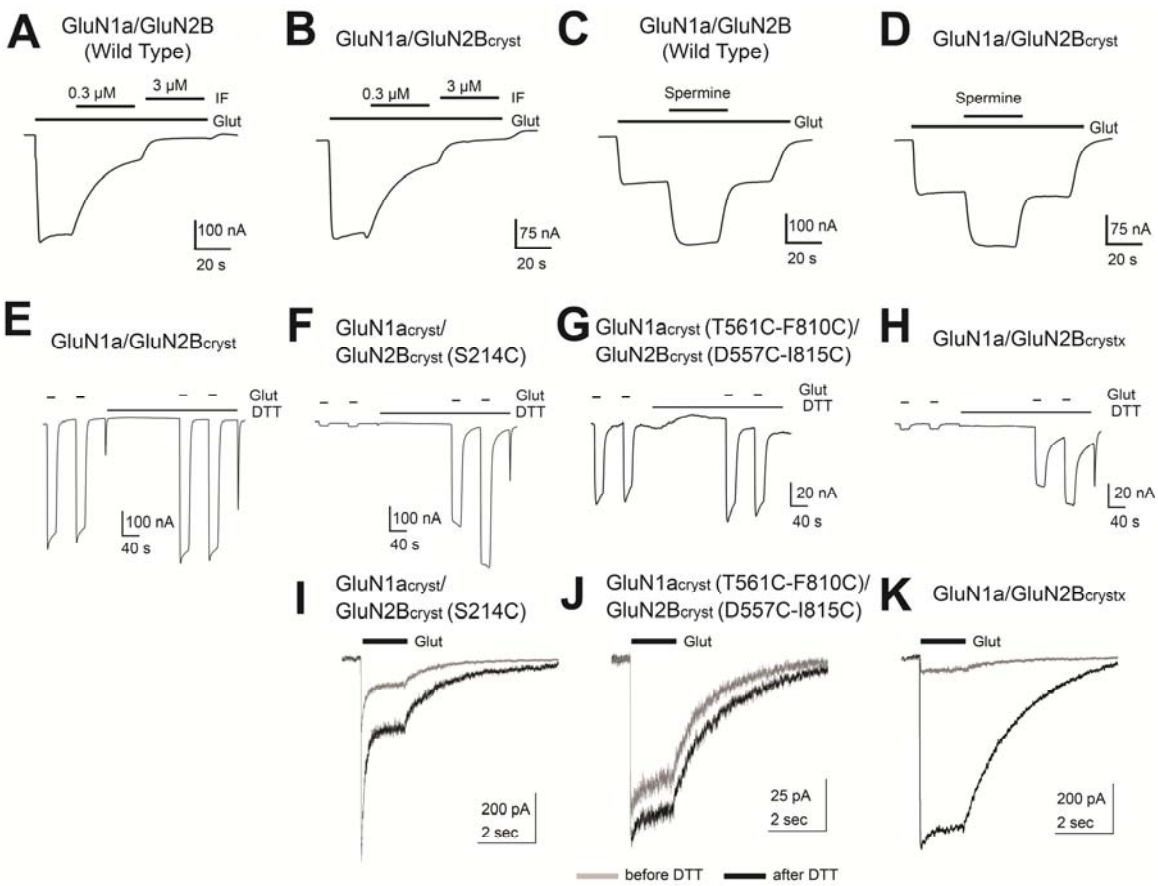

Fig. S6: Electrophysiological properties of GluN1a/GluN2B NMDA receptor mutants. (A and **B)** Allosteric inhibition of the wild-type **(A)** and GluN1a/GluN2B$_{cryst}$ **(B)** NMDA receptors by two different concentrations of ifenprodil (IF). Glut represents 100 μM of L-glutamate. **(C** and **D)** Potentiation of Glut-induced currents in the wild-type **(C)** and GluN1a/GluN2B$_{cryst}$ **(D)** NMDA receptors by spermine (100 μM). The patterns of both ifenprodil mediated allosteric inhibition and spermine mediated potentiation are similar between the wild-type and GluN1a/GluN2B$_{cryst}$ NMDA receptors indicating the physiological relevance of the mutant construct. **(E** to **H)** Redox experiments using two-electrode voltage clamp on *Xenopus* oocytes injected with cRNAs for GluN1a/GluN2B$_{cryst}$ NMDA receptors **(E)**, GluN1a/GluN2B$_{cryst}$ (Ser214Cys) NMDA receptors **(F)**, GluN1a$_{cryst}$-Thr561Cys-Phe810Cys/GluN2B$_{cryst}$-Asp557Cys-Ile815Cys **(G)**, and GluN1a/GluN2B$_{crystx}$ NMDA receptors (equivalent to GluN1a$_{cryst}$ Thr561Cys-Phe810Cys/GluN2B$_{cryst}$ Ser214Cys-Ile815Cys-Asp557Cys) **(H)**. There is little or no change upon addition of 2 mM of DTT in GluN1a/GluN2B$_{cryst}$ NMDA receptors whereas the major potentiation in GluN1a/GluN2B$_{cryst}$ (Ser214Cys) and GluN1a/GluN2B$_{crystx}$ NMDA receptor is observed. The current for GluN1a/GluN2B$_{crystx}$ NMDA receptor is typically small compared to that for GluN1a/GluN2B$_{cryst}$ NMDA receptors likely caused by inefficient surface expression in *Xenopus* oocytes. **(I-K)** The redox experiment done by whole-cell patch clamp on HEK293 cells expressing GluN1a/GluN2B$_{cryst}$ (Ser214Cys) NMDA receptors **(I)**, GluN1a-Thr561Cys-Phe810Cys/GluN2B$_{cryst}$-Ile815Cys-Asp557Cys **(J)**, and GluN1a/GluN2B$_{crystx}$ NMDA receptors **(K)**. In all of the cases, wash buffer contained 100 μM of glycine.

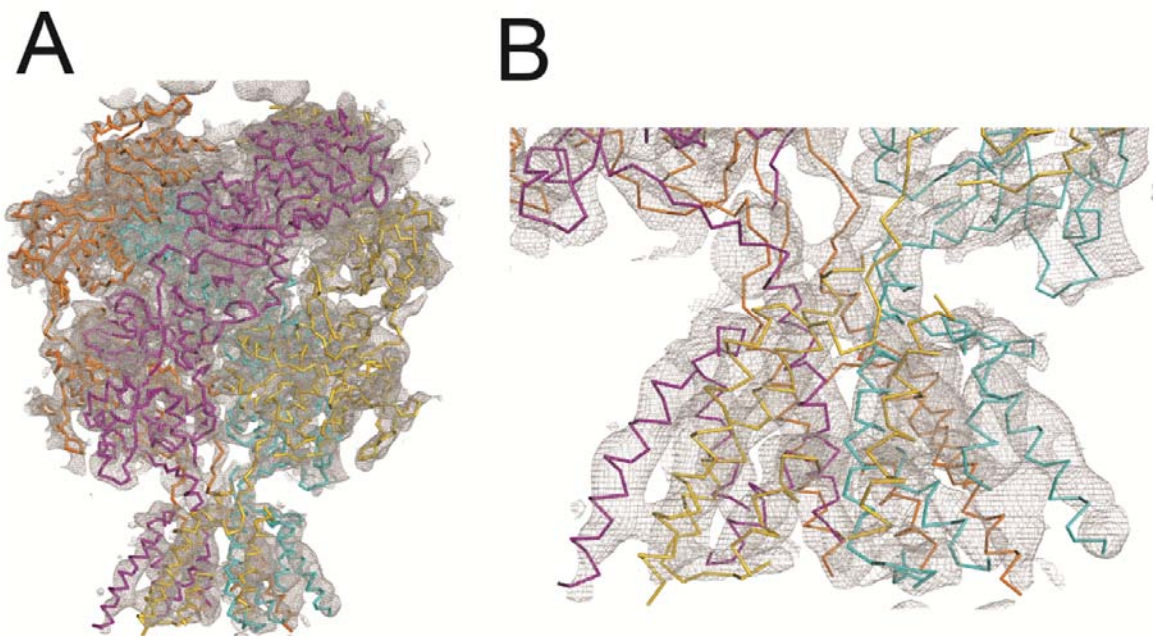

Fig. S7: Electron density maps of GluN1a/GluN2B$_{cryst}$ (non-cross-linked). (A) 2FoFc map calculated using the 5.7 Å x-ray diffraction data from the GluN1a/GluN2B$_{cryst}$ crystal is contoured at 1 σ and shown as grey mesh over the Cα trace of GluN1a/GluN2B$_{crystx}$ structure. Electron density clearly shows that incorporation of cross-linking mutations did not cause a major change in overall GluN1a/GluN2B structure. **(B)** The close up view of the TMD from *panel A*.

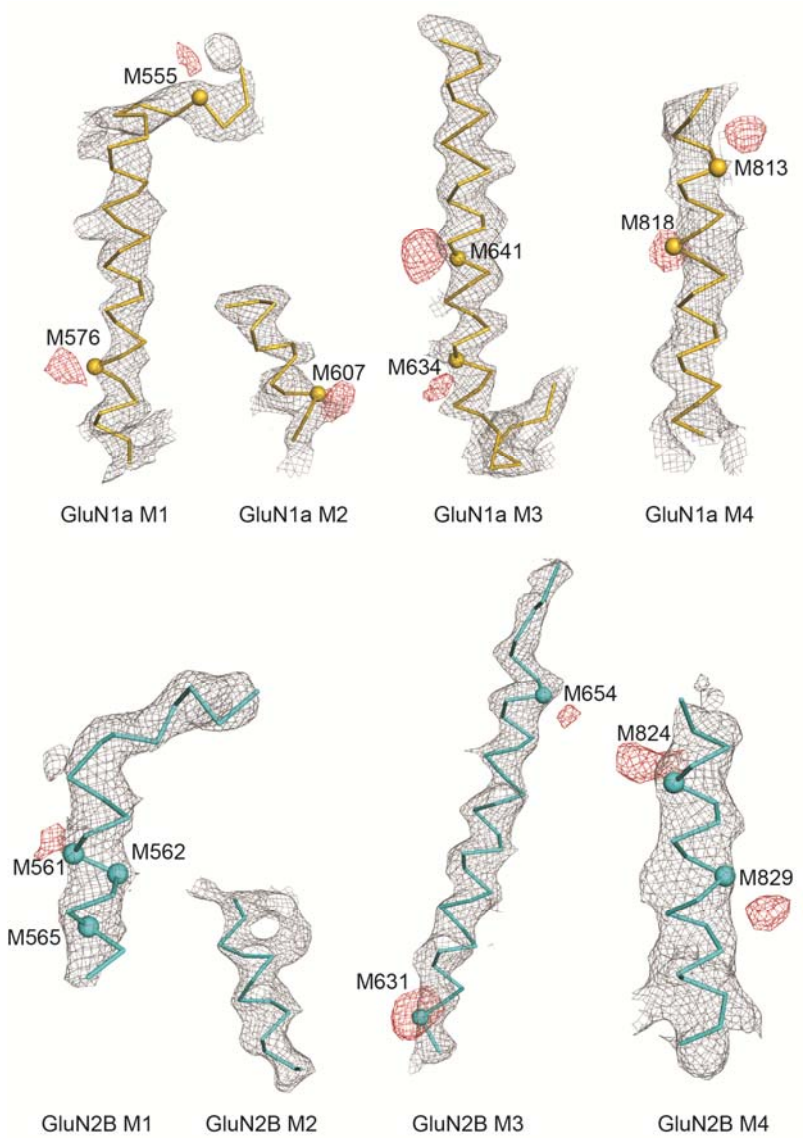

Fig. S8: Electron densities in the transmembrane domains in GluN1a/GluN2B$_{crystx}$. 2FoFc maps for the M1, M2, M3 and M4 helices of both GluN1a (α) and GluN2B (β) TMDs are prepared with a B-factor sharpening factor of -90 Å^2, countered at 1.0 σ and shown as grey mesh. The models of GluN1a (α) and GluN2B (β) are shown as yellow and cyan Cα traces, respectively. Cαs of methionine residues are shown as spheres. Anomalous difference Fourier maps calculated from data collected on two different selenomethionine-derivative crystals are averaged around the 2-fold non-crystallographic axis using COOT (43) and shown as red mesh. The maps are contoured at the following σ levels; 2.8 σ for GluN1a Met 555, 3.6 σ for GluN1a Met 576, 2.5 σ for GluN1a Met 607, 2.5 σ for GluN1a Met 634, 4.2 σ for GluN1a Met 641, 3.3 σ for GluN1a Met 813, 2.7 σ for GluN1a Met 818, 2.5 σ for GluN2B Met 561, 2.8 σ for GluN2B Met 631, 2.5 σ for GluN2B Met 654, 3.0 σ for GluN2B Met 824 and 2.5 σ for GluN2B Met 829. No significant signal was observed for residues GluN2B Met 562 and Met 565.

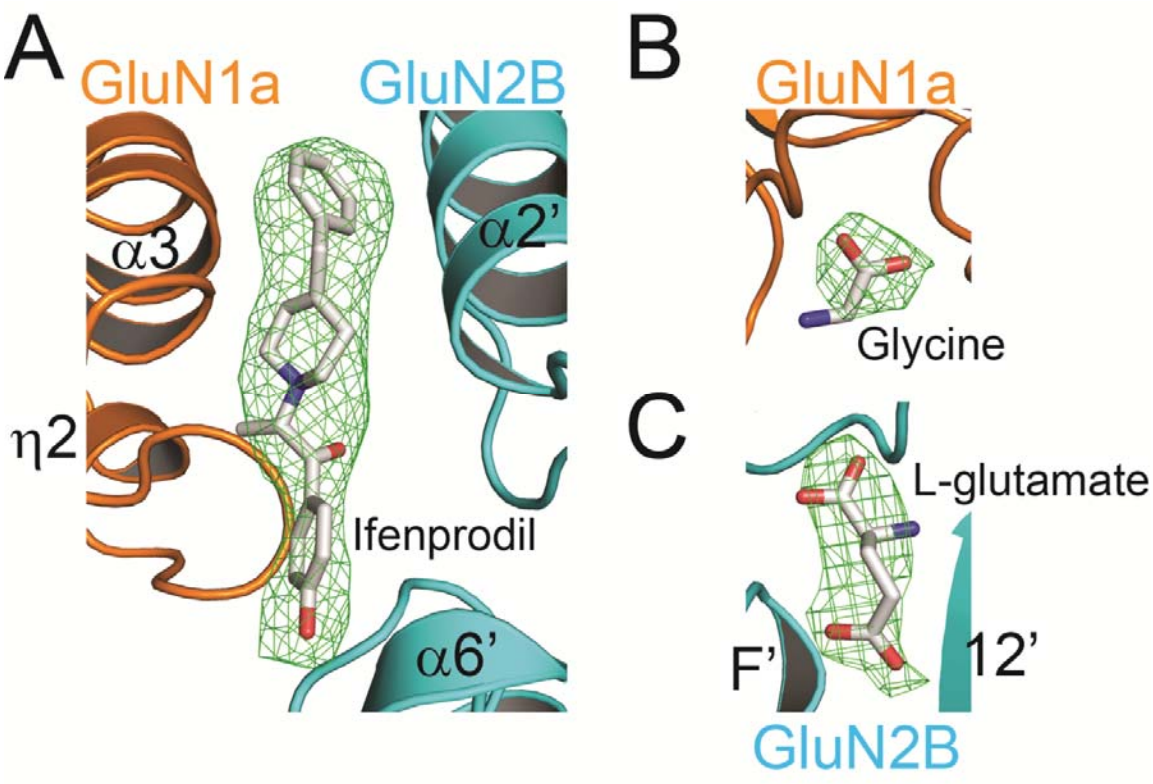

Fig. S9: Electron density maps for the ligands. FoFc electron density maps for the three ligands, ifenprodil **(A)**, glycine **(B)** and L-glutamate **(C)** at their respective binding sites are shown as green mesh and contoured at 4, 3 and 3 σ levels, respectively. Ligands are shown as light grey sticks.

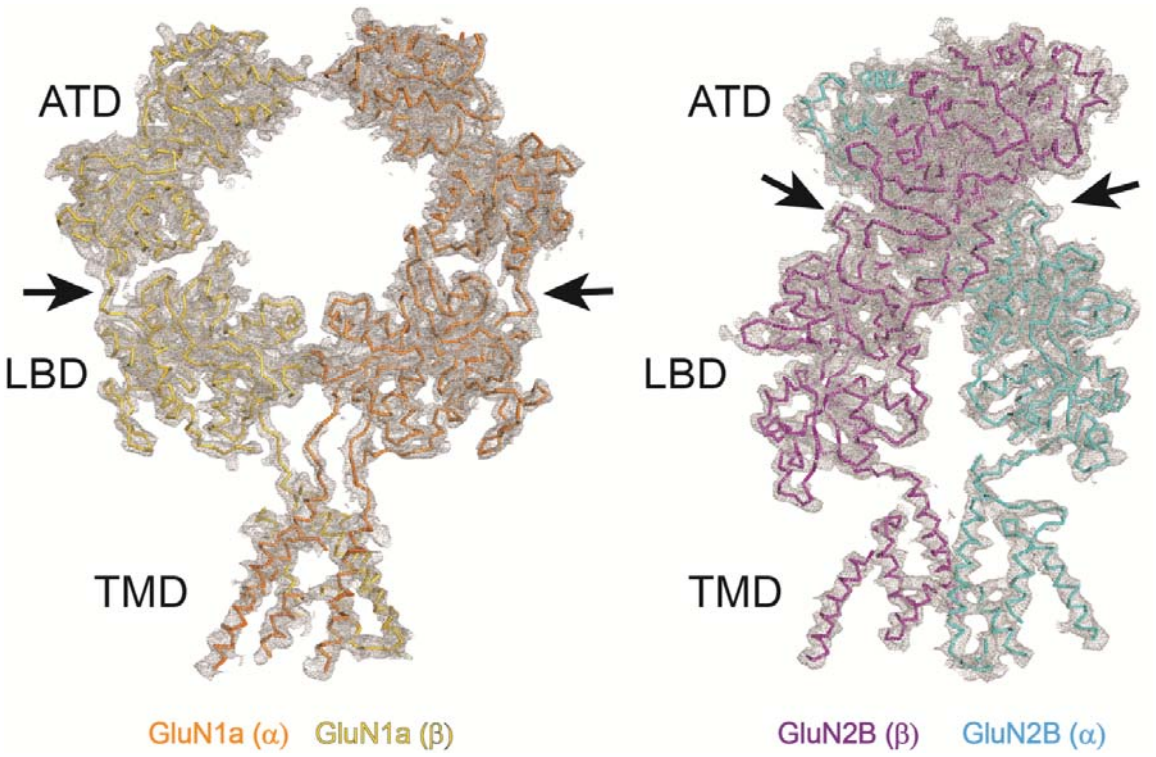

Fig. S10: Electron density maps for GluN1a/GluN2B$_{crystx}$. 2FoFc electron density maps for GluN1a$_{crystx}$ (left) and GluN2B$_{crystx}$ (right) subunits are show as grey mesh and countered at 1 σ. Maps are sharpened by a B factor of -90 Å^2. Cα traces for GluN1a (left) and GluN2B (right) subunits are shown. Note the distal and proximal positioning of the ATD-LBD linkers for GluN1a and GluN2B, respectively, as pointed with arrows.

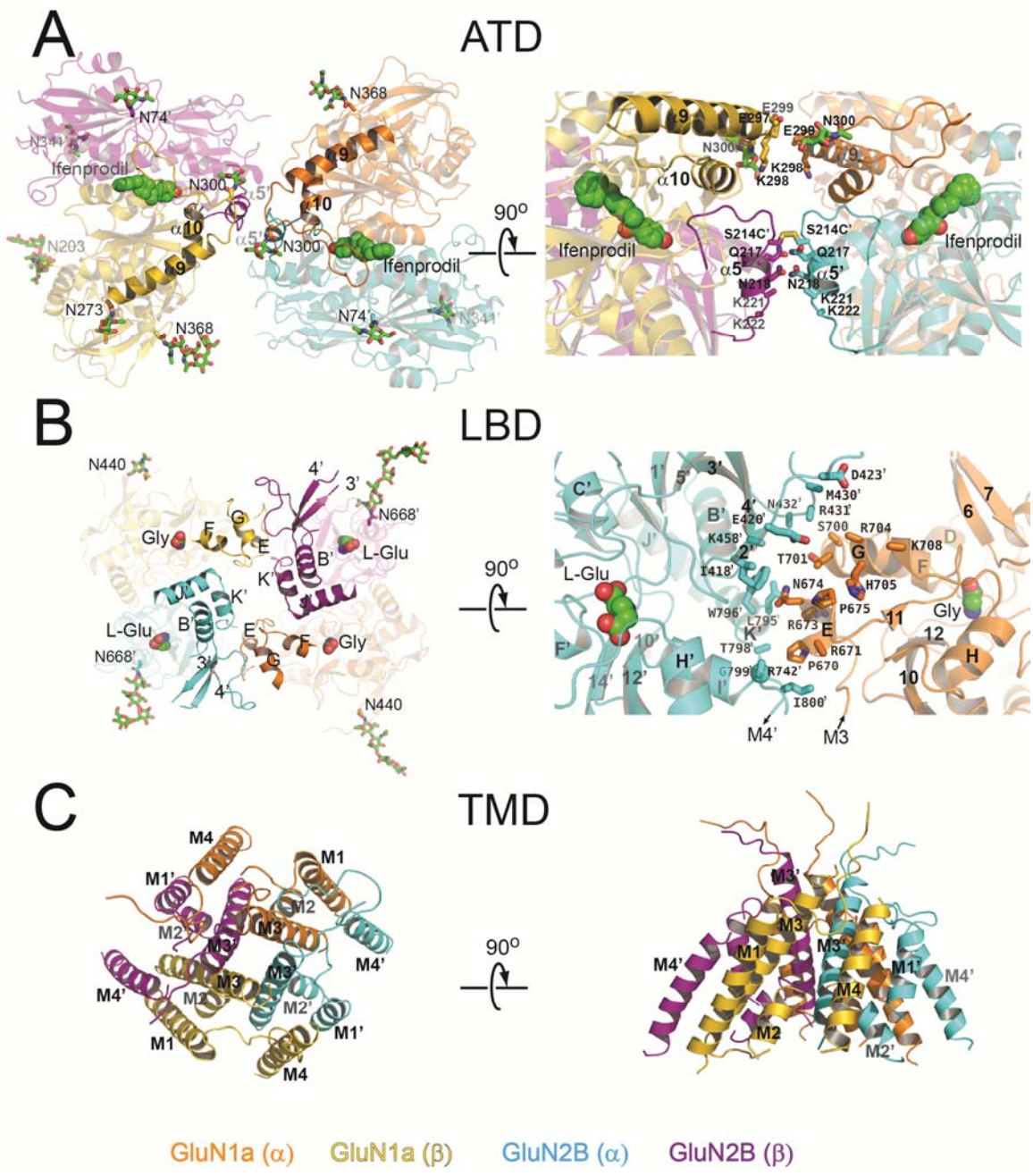

Fig. S11: Dimer-of-dimers assembly of GluN1a/GluN2B NMDA receptors. Tetrameric arrangement of ATD (**A**), LBD **(B)** and TMD **(C)** of GluN1a/GluN2B$_{crystx}$ NMDA receptors viewed from top (left panels) and side (right panels). Regions at the dimer-of-dimers interfaces are highlighted and residues in close proximity at ATD and LBD are shown as sticks on the side view. Side view of LBD (panel B, right) is one (between GluN1a (α) and GluN2B (α)) of the two equivalent sites of dimer-of-dimers interaction at LBD.

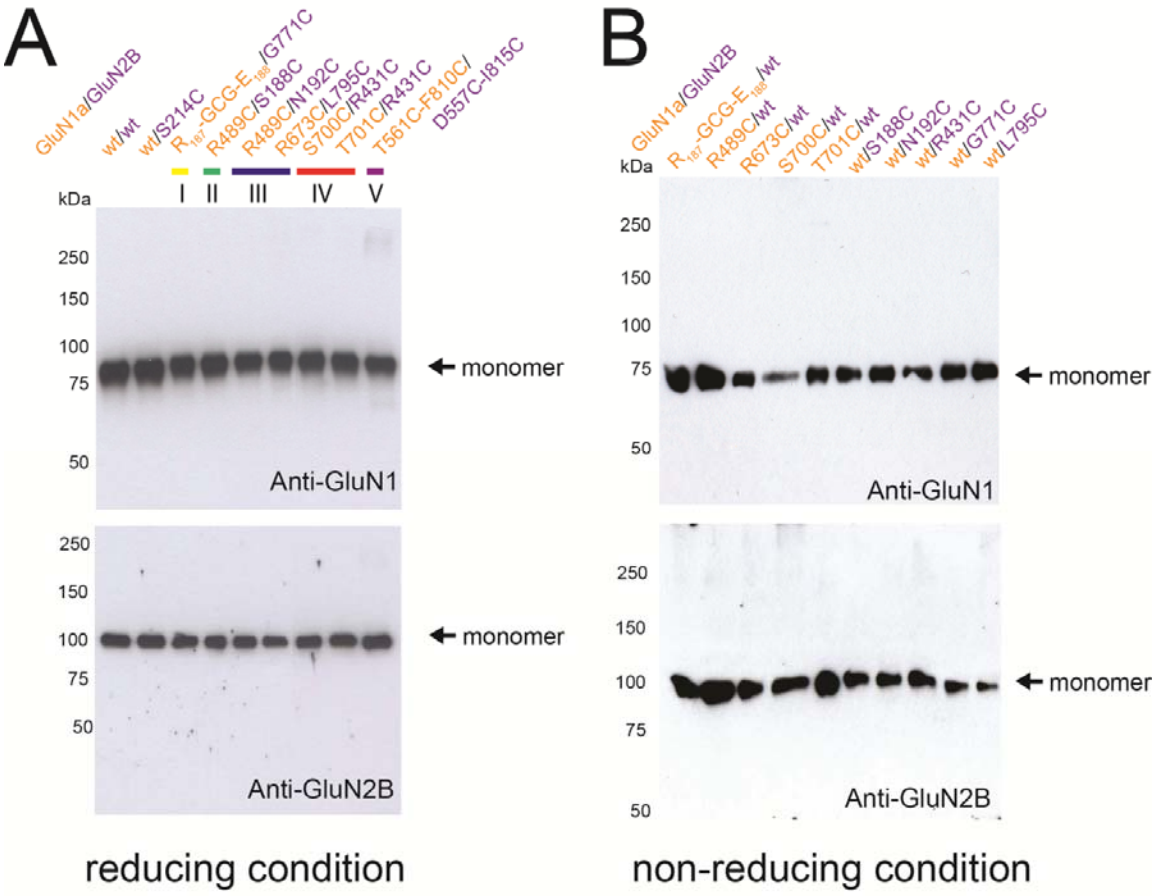

Fig. S12: Probing inter-subunit interfaces in GluN1a/GluN2B NMDA receptors. (A) Western blot analysis of spontaneous disulfide cross-linking of cysteine substituted GluN1a/GluN2B$_{cryst}$ NMDA receptors probed by anti-GluN1 (top) and anti-GluN2B (bottom) antibodies under reducing conditions. (**B)** Western blot analysis of wild-type (wt) GluN1a$_{cryst}$ / cysteine substituted GluN2B$_{cryst}$ and cysteine substituted GluN1a$_{cryst}$ / wt GluN2B$_{cryst}$ NMDA receptors probed by anti-GluN1 (top) and anti-GluN2B (bottom) antibodies under non-reducing conditions. Arrows indicate positions of the monomers.

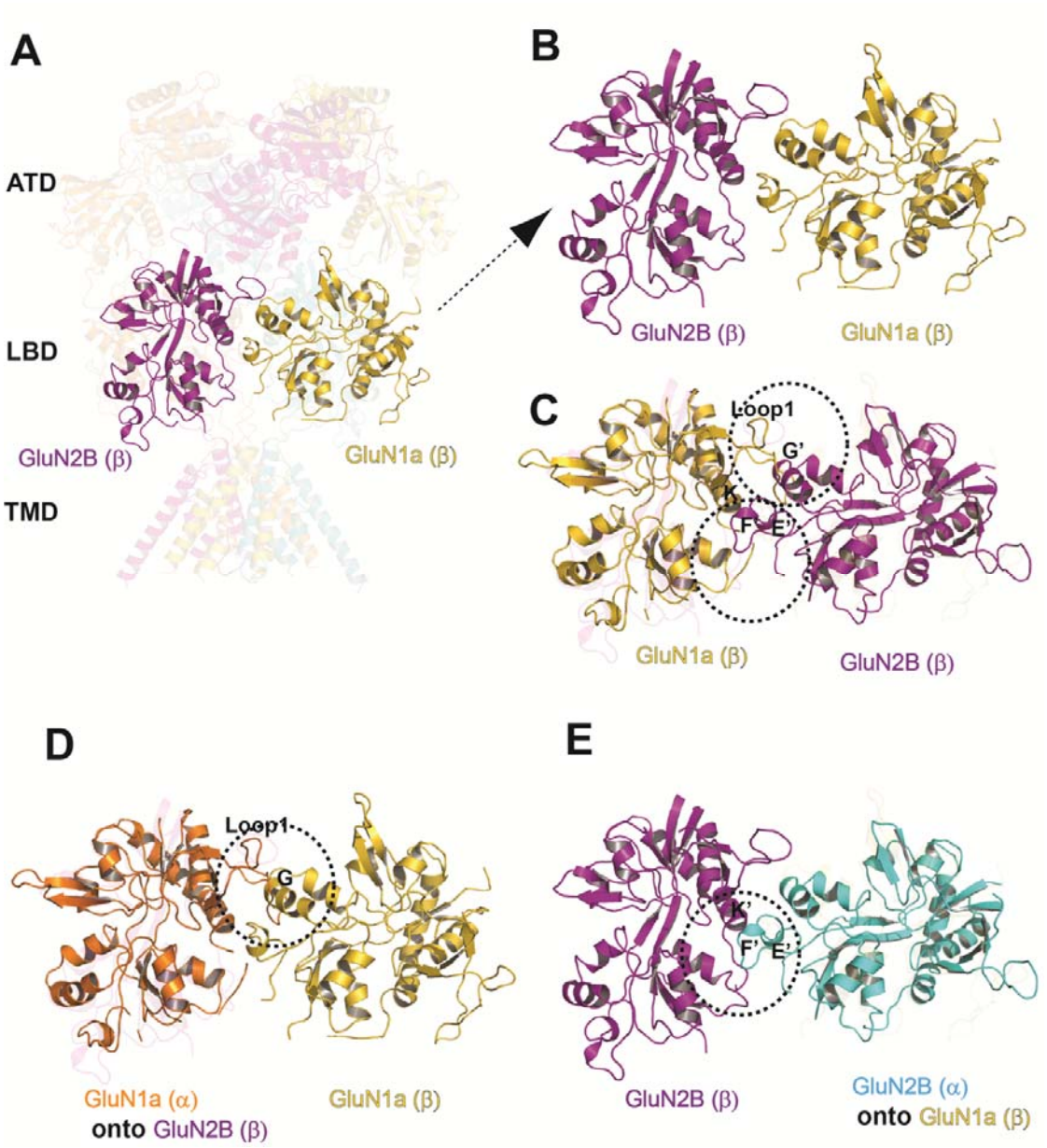

Fig. S13: Assessing various patterns of subunit arrangements at LBD. (A and **B)** Arrangement of GluN1a (β) and GluN2B (β) in the 1-2-1-2 arrangement observed in the crystal structure. **(C)** Swapping GluN1a and GluN2B to make 2-1-2-1 arrangement results in the clashes between GluN1a Loop 1 and GluN2B Helix G' and between GluN1a Helix K and GluN2B Helix E' and F' (dashed circles). **(D** and **E)** Superposition of GluN1a onto GluN2B **(D)** or GluN2B onto GluN1a **(E)** to enforce 1-1-2-2 arrangement causes clashes between GluN1a Loop 1 and GluN1a Helix G and between GluN2B Helix E', F' and K' (dashed circles).

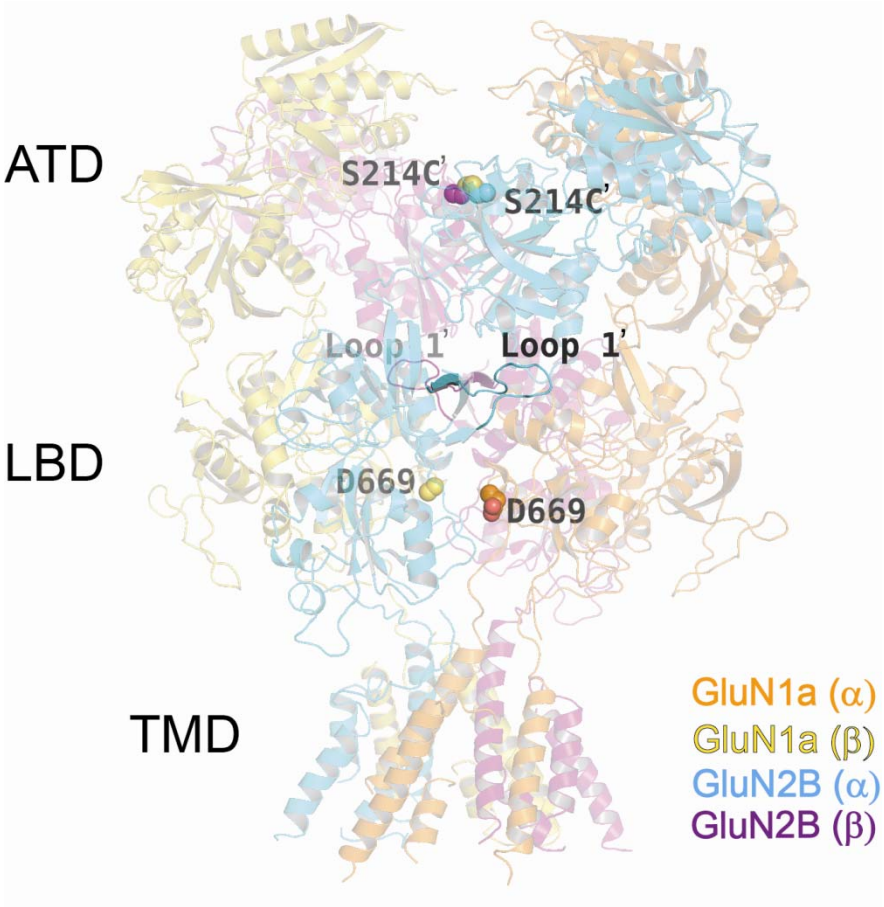

Fig. S14: Functionally critical elements located at the dimer interface of the GluN1a/GluN2B heterodimers. The critical sites at the extracellular region (GluN1a Asp 669 and GluN2B Ser214Cys' and Loop 1') where mutations have significant implication in function are highlighted and labeled on the overall structure of GluN1a/GluN2B NMDA receptors.

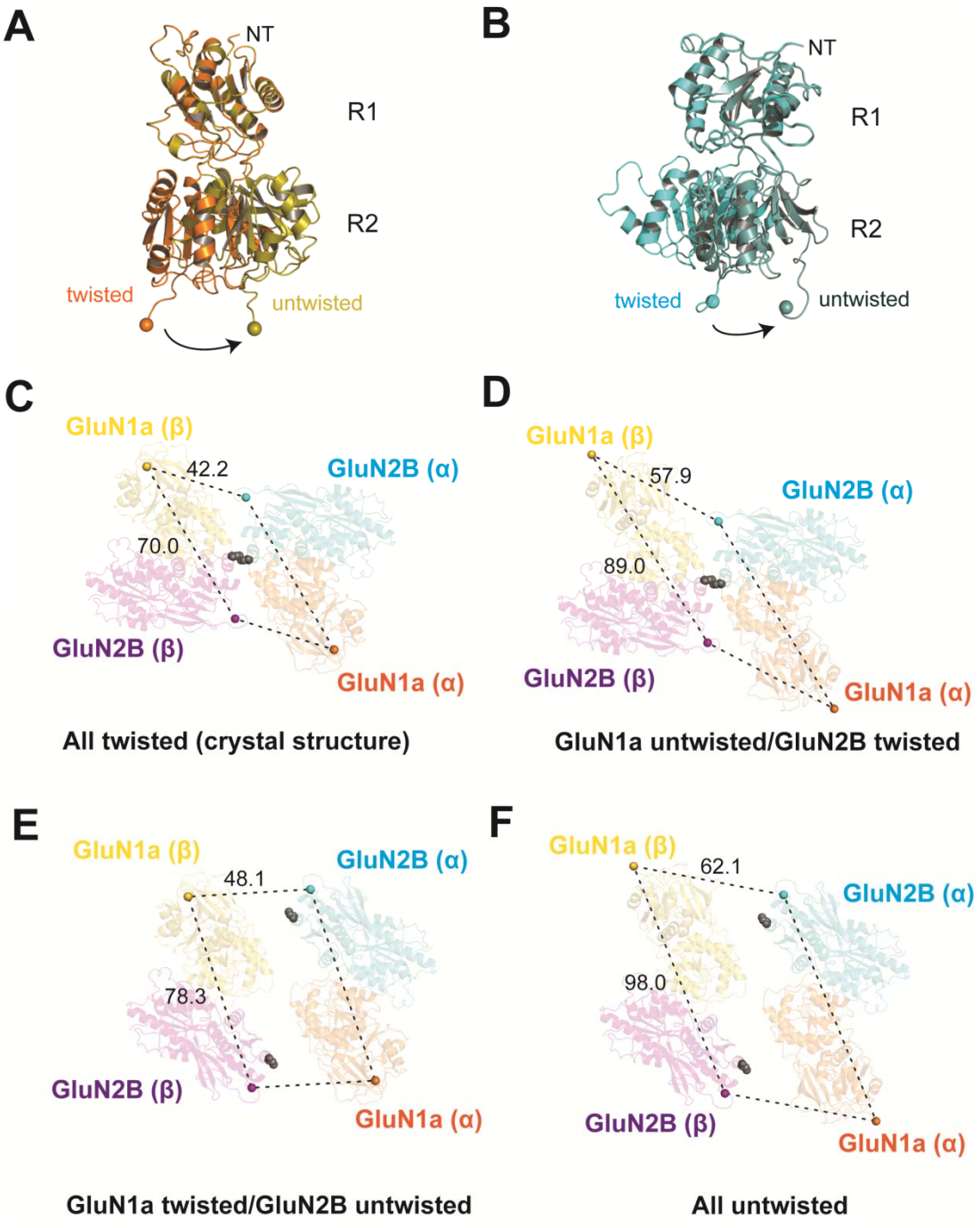

Fig. S15: Plausible changes in ATD conformation move the location of LBDs. (A-B). We make an assumption that the bilobed structures of ATD twist and untwist between the two lobes, R1 and R2, as previously reported (*28*). Untwisting of GluN1a **(A)** and GluN2B **(B)** by ~40° is accomplished by rotating R2 (lower lobe tethered directly

to LBD) using GluK1 ATD structure (*30*) as a guide. **(C** to **F)** Shown here are structures of ATD tetramers viewed "up" from the LBDs. The ATDs in the current crystal structure and the previously published GluN1b/GluN2B ATD structures have "twisted" conformations in both GluN1 and GluN2B **(C)**. Untwisting of GluN1a **(D)**, GluN2B **(E)**, or both **(F)** dramatically changes the location of LBDs. Numbers next to the dashed lines represent distance (in Å) between the beginning points of LBD defined as the Cαs of GluN1a Thr396 and GluN2B His405 (spheres). Note that untwisting of both GluN1a and GluN2B ATDs result in separation of the LBDs in both length and width to significantly more extent in GluN1a than GluN2B. This separation likely results in rearrangement of subunits within and between the GluN1a/GluN2B LBD thereby affecting patterns of ion channel gating. Shown in gray spheres are GluN2B Ser214 residues from both GluN2B (α) and (β). Formation of a disulfide bond by the GluN2B Ser214Cys mutation at the lower lobe (R2) not only traps the inter-subunit arrangement between the two GluN2B subunits, but also movement in the GluN2B ATD lobes.

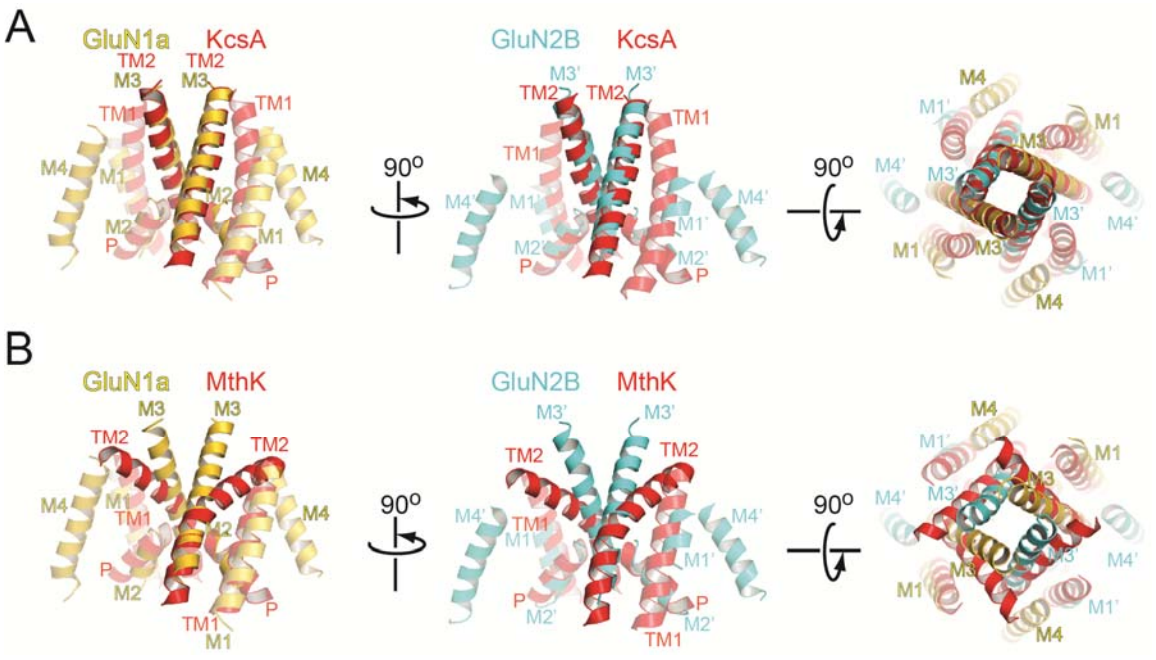

Fig. S16: Structural comparison of NMDA receptor ion channel with potassium channels. TMDs of GluN1a subunits (yellow, left panel) and GluN2B subunits (cyan, middle panel) are superposed onto the ion channel domains (red) of the closed conformation of KcsA (PDB ID: 1K4C) **(A)**, open conformation of MthK (PDB ID: 3LDC) **(B)**. The superposed structures are viewed from the side (left and middle panels) or from the extracellular side (right panel). Superposition is performed using Secondary-structure matching (SSM) tool. Loops are excluded from the figure for clarity.

Table S1. Data collection and refinement statistics

	GluN1a/ GluN2B cryst	GluN1a/ GluN2B crystx	GluN1a/ GluN2B crystx SeMet-1	GluN1a/ GluN2B crystx SeMet-2	GluN1a/ GluN2B crystx Ho^{3+}	GluN1a/ GluN2B crystx Gd^{3+}
Data collection						
Beamline	BL41XU (Spring-8)	23ID-B/D (APS)	23ID-D (APS)	23ID-D (APS)	23ID-B (APS)	23ID-B (APS)
Space group	$P2_1$	$P2_1$	$P2_1$	$P2_1$	$P2_1$	$P2_1$
Wavelength (Å)	1.0332	1.0332	0.9794	0.9794	1.5357	1.7111
Cell dimensions						
a, *b*, *c* (Å)	118.6, 164.3, 163.2	116.8, 163.2, 163.1	118.6, 164.3, 163.8	118.7, 162.9, 163.4	119.4, 164.1, 163.9	119.7, 164.3, 164.1
β (°)	95.0	93.8	93.9	94.0	93.1	93.0
Resolution (Å)	50-5.7 (5.9)	50-3.95 (4.09)	50-6.0 (6.21)	50-4.8 (4.97)	50-7.5 (7.77)	50-7.8 (8.08)
R_{merge}	0.1 (>1.0)	0.087 (>1.0)	0.078 (0.74)	0.077 (0.62)	0.09 (0.76)	0.082 (0.57)
$I/\sigma I$	7.9 (1.4)	9.3 (1.02)	10.1 (1.6)	8.5 (1.3)	9.1 (1.2)	10.6 (1.6)
Completeness (%)	99.2 (100)	98.6 (99.4)	99.5 (97.4)	96.7 (98.3)	87.3 (99.5)	93.1 (98.5)
Redundancy	3.7	3.8	3.8	2.0	1.8	2.0
Refinement						
Resolution (Å)		30.0-3.96				
No. reflections		52,162				
R_{work} /R_{free}		25.6/29.5				
No. atoms		20,246				
B-factors		202.8				
R.m.s deviations						
Bond lengths (Å)		0.002				
Bond angles (º)		0.61				
Ramachandran statistics (%)*						
Favored		92.1				
Allowed		7.6				

Highest resolution shell is shown in parenthesis.

[*] Ramachandran statistics are calculated using Molprobity (*45*).